Measurement 181 (2021) 109600

Contents lists available at ScienceDirect

Measurement

journal homepage: www.elsevier.com/locate/measurement

Current divider-based nanosecond high current pulse measuring systems

Mikołaj Nowak [a,*], Kazimierz Jakubiuk [a], Daniel Kowalak [b], Marek Pikoń [a], Józef Czucha [a], Jacek Starzyński [c]

[a] Department of Electrical Engineering, Control Systems and Informatics, Faculty of Electrical and Control Engineering, Gdansk University of Technology, Gdansk, Poland
[b] Department of Mechatronics and High Voltage Engineering, Faculty of Electrical and Control Engineering, Gdansk University of Technology, Gdansk, Poland
[c] Electrical Engineering Faculty of Warsaw University of Technology and Military University of Technology, Warsaw, Poland

ARTICLE INFO

Keywords:
Current dividers
Current transducers
High current measurement
Computer simulation
Pulse current
Pulse-forming circuits

ABSTRACT

This paper presents the analysis of the new approach to the measurement methodology of significant values (in order of hundreds of kA) and huge steepness (in order of MA/μs) current pulses based on current dividers along with a comparison of the various types transducers suitability in measuring systems with such extreme parameters. Such dividers are used to extend the measurement ranges of current transducers with limited current conversion capabilities. The results of the selected current dividers field-circuit simulations have been presented, including their attributes and potential application as an important elements of the high-current measurement circuits. The physical prototypes of dividing systems have been verified using an experimental high-power pulse generation and forming system based on the flux compression generator and ultra-fast fuse-opening switch. As the additional aim of this study, the dividers current ratio error compensation method based on the general field-circuit model of current divider has been proposed.

1. Introduction

The measurements of high current pulses (in the order of hundreds of kA) and the slopes duration in the ns order occurring in many specific research systems, such as surge current generators [22,34], flux compression generators (FCG) with pulse forming systems [19,24,49], high power Marx generators etc., brings many difficulties. The current transducers available on the market do not always have the appropriate metrological properties. The high bandwidth Rogowski coils, popular in the scientific community [2,10,29,32,36,38,41,43–45,56], have large measuring ranges, but are not sufficiently resistant to the interferences occurring in the tested systems, in particular in high-voltage systems, due to disturbing signals transmitted by electrical couplings and easily induced in transducers with high self-impedance. Therefore, it is essential to use transducers with a similarly wide bandwidth but low internal impedance, a high level of carrier signal in relation to the interfering signal and effective shielding systems. The current transducers commonly used in the measurement of pulse currents and meeting the above criteria are, for example, the Pearson current transformers [6,33], which in general have appropriate metrological attributes but for the required frequency response commercially available models do not provide adequate conversion ranges due to many technical limitations. Thus, there is a need to increase their measuring range.

One of the ways is to use the so-called current divider in the main measuring path. The apparently simple operating principle of the current divider consists of the physical division of the current path into N parallel paths and measuring the current about $i(t)/N$ in one of them. An important condition for minimizing the measurement error is that the current distribution in individual paths is practically independent of the frequency (or pulse steepness) in the entire spectrum of the measured current pulses. This requirement cannot be fulfilled by dividing the main current into two or more parallel paths with different parameters (impedances), allowing the current to be divided into parts $i(t)\ (N-1)/N$ and $i(t)/N$. In this case, the distribution of current depends significantly on the frequency. Hence, the key steps are to equalize the current distribution in each successive current path. Unfortunately, in the practice of using this type of current dividers, actions aimed at equalizing the current density in individual traces, due to the complex geometries of the measurement systems, are difficult.

* Corresponding author at: Faculty of Electrical and Control Engineering, Gdansk University of Technology, 11/12 Gabriela Narutowicza ST, 80-233 Gdansk, Poland.
E-mail addresses: mikolaj.nowak@pg.edu.pl (M. Nowak), kazimierz.jakubiuk@pg.edu.pl (K. Jakubiuk), daniel.kowalak@pg.edu.pl (D. Kowalak), mpikon@wp.pl (M. Pikoń), jozef.czucha@wp.pl (J. Czucha), jstar@ee.pw.edu.pl (J. Starzyński).

https://doi.org/10.1016/j.measurement.2021.109600
Received 25 February 2021; Received in revised form 22 April 2021; Accepted 13 May 2021
Available online 29 May 2021

The paper presents a brief review of the effectiveness of typical high-current transducers solutions for measuring extreme current pulses as a justification for the use of range-extending pulse current dividers. Two prototypes of pulse current dividers have been proposed and a series of simulation tests and static measurements have been carried out for them, based on which a theoretical circuit-based model of the current divider has been created. The new method for compensating the total current ratio error based on the proposed model has also been introduced. The properties of a representative plate current divider prototype and the presented method of error compensation have been verified experimentally with current pulses generated by the FCG and the ultra-fast fuse-based pulse-forming circuit.

2. Justification for the use of pulse current dividers

Various methodological solutions for measuring high-value currents have long found their place in the literature [7,39,46]. However, due to the unusual requirements for the bandwidth, range and noise immunity of the transducers, only some measurement methods have been selected for analysis. Those requirements have been developed on the basis of a representative current waveform of a FCG with a fuse-based pulse-forming system, obtained during field tests of the device. The waveform of the current breaking with a steepness exceeding 350 kA/μs along with its amplitude spectrum has been shown in Fig. 1. The principle of FCG operation has been detailed in [49].

To measure short-circuit and surge currents in laboratory systems, high-current shunts [8,18,26,47] with a specific resistance made in the form of connected coaxial pipe sections are commonly used. Unfortunately, in the case of shunts with measuring ranges of hundreds of kA, it is impossible to provide them with an adequate bandwidth (the standard bandwidth reaches hundreds of kHz). Typical, laboratory versions of this type of shunts (manufactured at the Gdańsk University of Technology) together with the measured gain and phase error characteristics have been shown in Fig. 2.

However, the most important feature that excludes the use of high-current shunts for transient currents measurement in systems with

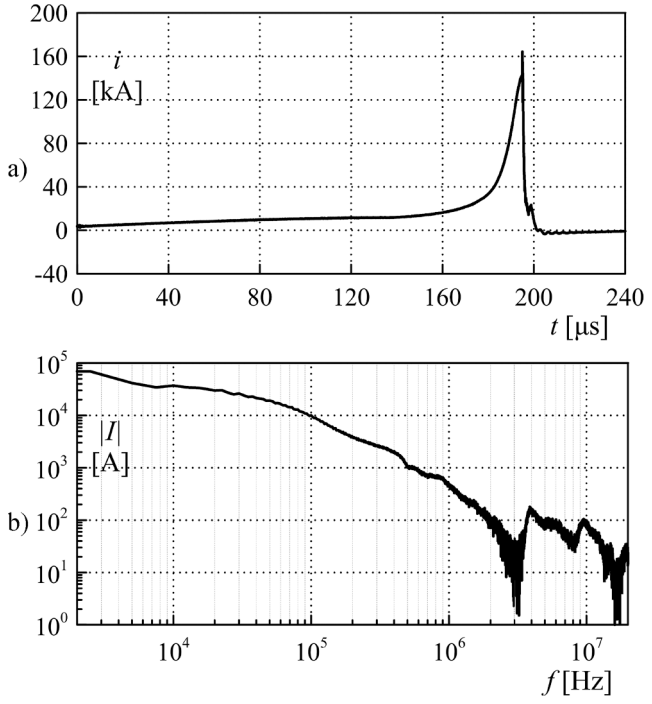

Fig. 1. Representative experimental a) current waveforms, and b) current amplitude continuous spectrum of the impulse forming system with FCG and high speed fuse-opening switch.

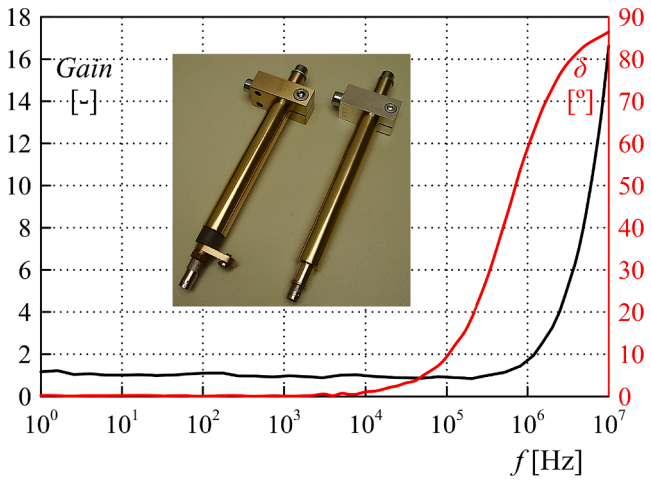

Fig. 2. Frequency characteristics of the pulse current shunt gain and phase error.

extreme impulse parameters is the lack of galvanic separation of the transducer from the rest of the measuring setup. For example, in the case of a fuse-based high-power pulse forming systems [19,24], a voltage drop of 30 to 50 kV with respect to the reference ground may appear on a fragment of the current path with a length of approximately 100 mm. Direct transfer of such voltage even to a safeguarded oscilloscope input may result in the loss of recorded data or even damage to the equipment and danger of electric shock for the personnel.

The transducer ensuring the galvanic separation of the measuring equipment from high potentials occurring in systems with current pulses of high steepness and amplitude is the Rogowski coil [29,32,36,41,43–45,55–56], which also provides a satisfactory frequency response and conversion range in appropriate design versions [2,16,25,45]. However, the Rogowski coil, due to the low level of magnetic coupling, requires a significantly expanded secondary winding, which causes an increase in the impedance of the transducer and its susceptibility to electrically transmitted interferences. At the same time, it is necessary to use an additional electronic integrator that can increase the susceptibility to interference and requires low amplitude input signals, or additional numerical processing of the signal.

Another usable transducer with a similarly wide frequency band, but at the same time ensuring low self-impedance (through the use of distributed resistive winding termination [33]), guaranteeing strong attenuation of electrical interferences is the Pearson current monitor (PCM). An additional advantage of this measuring transformer is the feature of self-integration of the signal through a distributed RL network, which eliminates the need for additional, sensitive electronic circuits or further numerical postprocessing of the signal. Moreover, the implementation of a ferromagnetic core provides a lower sensitivity to the position of the current path in relation to the transducer window than in the case of Rogowski coils [25,43,50] and the possibility of using a winding with fewer turns. On the other hand, due to the saturation effect occurring even despite the demagnetization of the core by the secondary winding, this transducer provides lower measuring ranges.

A comparison of the same current waveform recorded with the above-mentioned galvanically separated transducers has been presented in Fig. 3. The noise occurring during the rising slope of the current visible in Fig. 3.a) and resulting from the process of closing FCG winding effectively prevents the analysis of the measurement results even with proper post-processing filtration. In the case of the Pearson current monitor, this phenomenon is suppressed to a significant extent (Fig. 3. b).

It is also possible to use significant values and a steepness pulse current measuring system based on the Faraday electro-optical phenomenon [36,40,52]. This solution meets all the previously mentioned

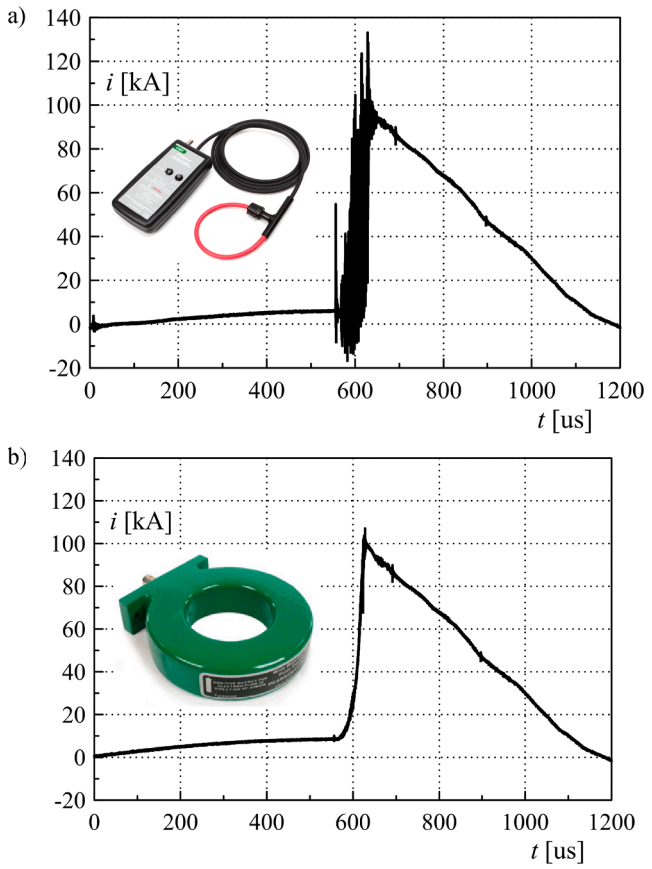

Fig. 3. Representative experimental current waveforms during the operation of the FCG registered with a) a Rogowski coil, and b) a Pearson current transducer including interference of the measurement signal.

metrological criteria, but due to the high degree of complexity, low availability on the market, high sensitivity to vibrations and mechanical displacements [40,52] and high processing errors compared to other measurement systems it has been rejected during the pre-selection process.

The last noteworthy solution is the measurement of the magnetic field of the structure of conductors with a specific geometry with the use of B-DOT type pulse probes [10,34,51]. Due to the high susceptibility of this type of solution to the conductor system magnetic field distribution, the need of the measurement calibration in case of a change in the conductor layout, the sensitivity of the measurement system to external fields and a relatively narrow measurement band concentrated in the high frequency range [34], the measurement method is not widely used during current measurement.

3. Current dividers

As a result of the analysis, the Pearson current monitor type transducer has been selected as the most suitable for measuring high-value and high-steepness currents generated by FCG and fuse-based pulse forming system. However, due to the insufficient measuring range because of core saturation [28,33] (either by current DC component or current–time product $\int_0^t i d\tau$) or exceeding the safe range of the output voltage of the available transducer models with a sufficient bandwidth (20 MHz), it is necessary to extend its range by dividing the main circuit current.

The current divider error in relation to the reference value depends to a large extent on the mutual correlation of the individual current paths impedances. In the low-frequency range, the resistances of individual paths play a dominant role in the distribution of current, while above the first pole of the frequency response, the inductive distribution of the current becomes decisive. Hence, the uneven distribution of current in branches with significantly different impedances introduces a strong frequency-dependent system non-linearity. Thus, the only method of ensuring a reasonably constant frequency conversion characteristics is to ensure the uniform current flow in all divider paths.

The presented measurement method was designed for implementation in a pulse generation and forming system based on an FCG and an ultra-fast fuse-opening switch. Due to the extreme current breaking steepness exceeding 350 kA/μs and voltage pulses exceeding 700 kV, a necessary condition for the used current divider topology is to minimize the need of introducing additional circuits which would increase the inductance of the proper main circuit of the generating system. Therefore, an obvious operation during the current divider construction is to use the naturally existing current paths in the system. An example of a divider structure consisting of four cylindrical spacers connecting two parallel construction plates is shown in Fig. 4. The presence of a pulse-forming system coil wound coaxially with the fuse requires its point connection to the upper structural plate, which makes it impossible to obtain a fully symmetrical current flow in the divider paths due to different distances from the coil end.

Fig. 5 shows the prototype of a cylindrical current divider made as two closely spaced rings (due to the need to limit additional inductance) placed coaxially on the fuse case. The left inset of Fig. 5 shows the path of the current measured by the main PCM.

This design has been created to test the maximum limitation of the measured current rise-time. For this purpose, a transducer with an extended bandwidth but an even more limited measurement range was used. Hence, the necessity of significant current division and the simultaneous ability to correct the number of parallel current paths.

4. Simulations of current flow in complex conductor systems

In order to analyze the pulse current flow in a complex array of conductors constituting the current divider, a series of simulation calculations has been performed using the finite element method. Geometric models of the plate and cylindrical current dividers implemented in the CST Studio [1] computing environment with created finite element meshes have been shown in Figs. 6 and 7. The models reflected

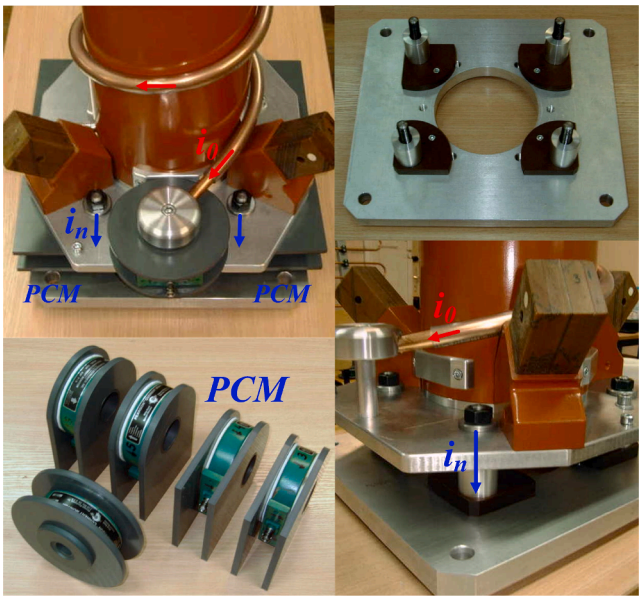

Fig. 4. Views of the physical model of a plate divider built into the construction of the high-power pulse generation and forming system, consisting of four cylindrical paths with Pearson current monitors. The current flow direction has been marked. PCM – Pearson current monitor.

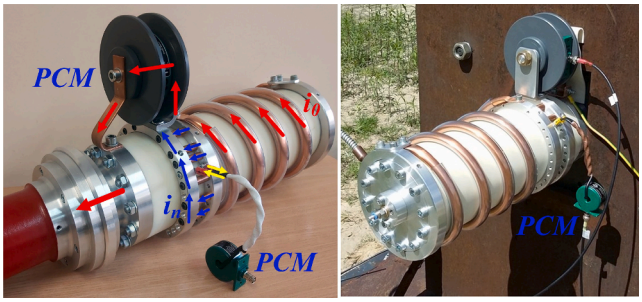

Fig. 5. Views of the physical model of a cylindrical divider built into the construction of the high-power pulse generation and forming system, consisting of up to 25 cylindrical paths. The current flow direction has been marked. PCM – Pearson current monitor.

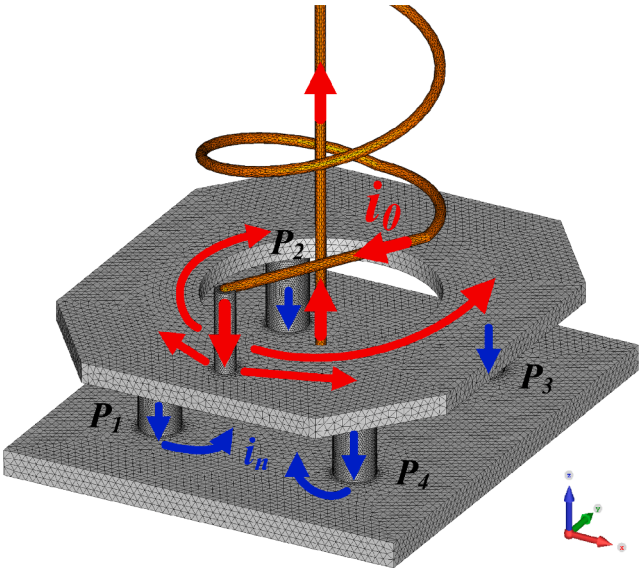

Fig. 6. View of the geometric model of four-path plate current divider with generated mesh of finite elements.

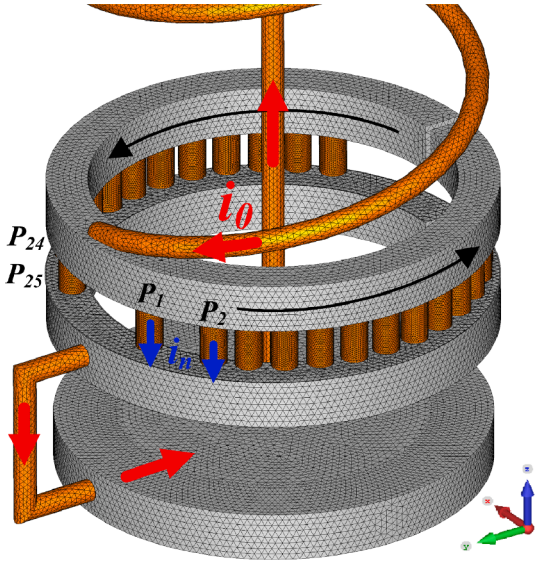

Fig. 7. View of the geometric model of twenty-five-path cylindrical current divider with created mesh of finite elements.

the actual designs. The realistic characteristics of construction materials for the current paths have been modelled.

On the contact surfaces of individual current paths with the divider's main path, simplified models of multi-point contacts have been created in the form of parallel connected lumped elements with specific transition resistances. In literature, there are a number of contact resistance models, the complexity of which depends strictly on the needs of the application and the permissible error limit [4–5,15,20,23,42,54]. In fact, the value of the contact resistance in high-current circuits is highly nonlinear as a function of the current value and the heat generated in the contacts, but for extremely fast transients it is possible to omit this type of considerations without introducing a significant calculation error [27,48]. A simplified model based on [14,17] has been used in the presented numerical systems. The approximate value of the contact resistance has been determined on the basis of the relationship (1)–(3).

$$R_p = R_{p1}/n \tag{1}$$

$$R_{p1} = \rho/2r_{p1} \tag{2}$$

$$r_{p1} = \sqrt{\frac{F}{\pi \xi H_B}} \tag{3}$$

where: R_p – contact transition resistance consisting of n parallel contact points with resistance R_{p1}, ρ - contact material resistivity, r_{p1} - radius of the equivalent contact surface of the point contact, F - contact pressure force (determined during assembly), H_B - contact material hardness according to Brinell (350 MPa for copper, 250 MPa for aluminium), ξ – coefficient of contacts elastic deformation (with a value of approx. 0.5 for a surface type contact).

In practice, however, it is impossible to obtain several current contacts with the same transition resistances, hence the contact resistance ratios of the individual current paths have been refined based on measurements of low-frequency current flow in relation to the main current of the divider. Based on preliminary analyses, it has been determined that a contact resistance calculation error of no more than 50% causes a resultant model error of less than 6% over the entire considered frequency band. This fact results from the limited influence of the contacts resistances on the divider current flow in relation to the remaining divider parts resistances, especially in the range of higher frequencies.

The models use appropriate open magnetic boundary conditions. The maximum elementary size of the discrete elements has been determined using the method of successive approximations until a satisfactory difference in the relative discretization error of the successive iterations has been achieved.

On the basis of simulations, the frequency-dependent current flow in the branches of current dividers for the plate and cylindrical versions has been determined. Visualizations of the current density module distribution in two versions of the dividers for significantly different excitation frequencies from the range of considered frequency band have been shown in Fig. 8 and Fig. 9.

For frequencies above approx. 100 Hz, a strong influence of the last turn of the pulse-forming system coil on the current flow in the divider paths is visible, depending on the mutually consistent or opposite direction of the current density vectors. A cross-sectional map of the normal component of the current density vector of both dividers is also presented in Fig. 10 and Fig. 11. The asymmetry of current flow due to the pulse forming system coil coupling is particularly well visible in Fig. 11 b).

The frequency characteristics of the dividers individual paths currents have also been determined and presented in Fig. 12 and Fig. 13. On the basis of these characteristics, it is possible to select and optimize the parameters of the equivalent circuit model of the dividers, which have been discussed later in this paper.

The design of the cylindrical current divider was intended to achieve high uniformity of current flow and to minimize the parasitic

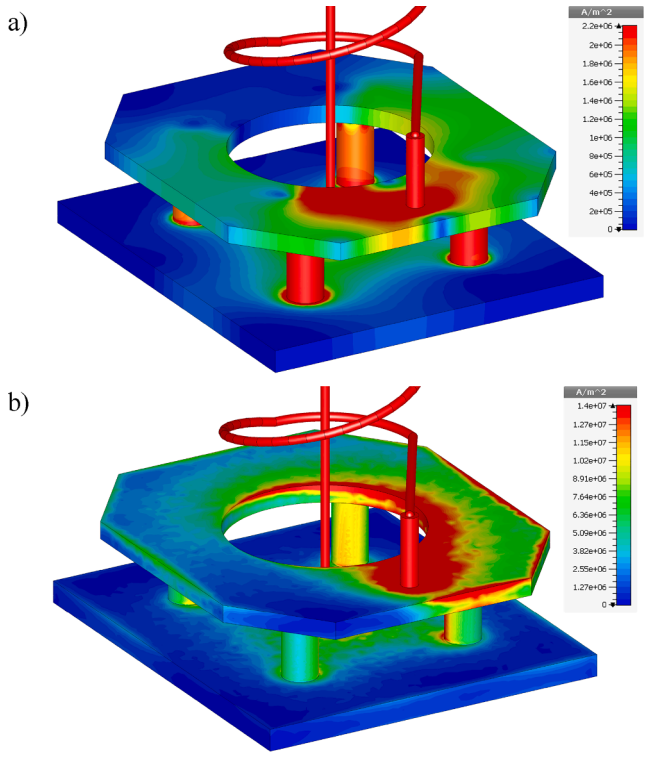

Fig. 8. Visualization of the current density module distribution in the plate divider model for the excitation frequency of a) 1 Hz, and b) 10 kHz.

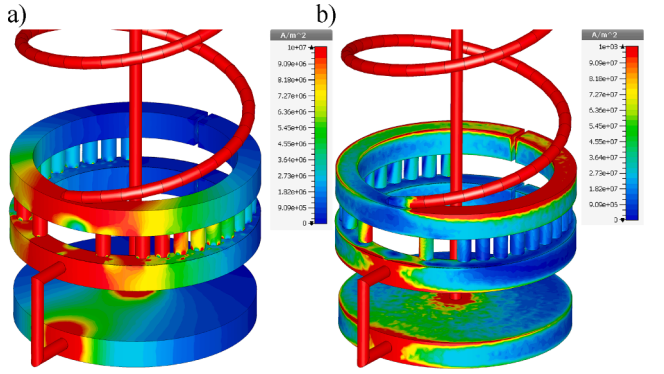

Fig. 9. Visualization of the current density module distribution in the cylindrical divider model for the excitation frequency of a) 1 Hz, and b) 10 kHz.

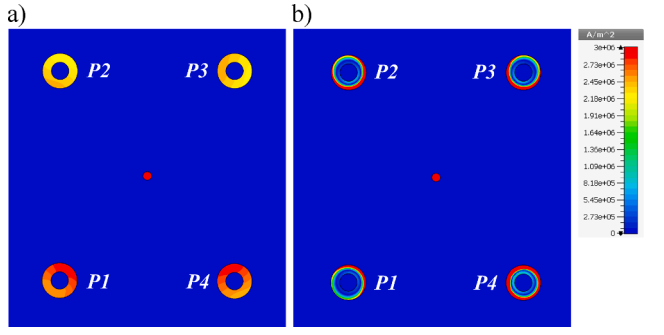

Fig. 10. Cross-sectional map of the current density vector normal component in the plate divider model four paths for the excitation frequency of a) 1 Hz, and b) 10 kHz.

inductances and resistances introduced into the measurement system. However, due to the significant coupling of the divider paths with the main current path and the concentrated connection point between the main current path and the divider ring, it is impossible to obtain a satisfactory symmetry. Moreover, simulation calculations show that current dividers with a large number of parallel paths generate higher current flow distortions while requiring a much more extensive numerical model for the compensation process. Therefore, the divider in the plate configuration (Fig. 6 and Fig. 8) has been chosen as the subject of further analysis.

5. Circuit-Model-Based algorithm of current dividers error compensation

In order to determine an accurate value of the total current of the measurement system from the current of a single divider path, it is necessary to consider its transfer characteristics and formulate a circuit model to compensate for the original current measurement. Fig. 14 presents a general model of the multipath current divider including the magnetic couplings between the main current conductors and individual divider paths, couplings between divider paths, contact resistances, and nonlinear series resistances. This paper contains representative results of measurements and model-based compensation performed with the use of a four-path plate divider (Fig. 4).

Equation (4) describes the universal model of a non-linear current divider. Vectors and matrices of the model coefficients for the 4-path divider have been presented in (5) and (6).

$$\boldsymbol{L}\frac{d}{dt}\boldsymbol{i}+\boldsymbol{R}\boldsymbol{i}=\boldsymbol{A}\frac{di_0}{dt}+\boldsymbol{B}i_0 \tag{4}$$

$$\boldsymbol{L}=\begin{bmatrix}(L_1-M_{12}) & (M_{12}-L_2) & (M_{13}-M_{23}) & (M_{14}-M_{24})\\ (M_{12}-M_{13}) & (L_2-M_{23}) & (M_{23}-L_3) & (M_{24}-M_{34})\\ (M_{13}-M_{14}) & (M_{23}-M_{24}) & (L_3-M_{34}) & (M_{34}-L_4)\\ 0 & 0 & 0 & 0\end{bmatrix} \tag{5}$$

$$\boldsymbol{i}=\begin{bmatrix}i_1\\ i_2\\ i_3\\ i_4\end{bmatrix};\boldsymbol{R}=\begin{bmatrix}R_1 & -R_2 & 0 & 0\\ 0 & R_2 & -R_3 & 0\\ 0 & 0 & R_3 & -R_4\\ 1 & 1 & 1 & 1\end{bmatrix};\boldsymbol{A}=\begin{bmatrix}M_{01}-M_{02}\\ M_{02}-M_{03}\\ M_{03}-M_{04}\\ 0\end{bmatrix};\boldsymbol{B}=\begin{bmatrix}0\\ 0\\ 0\\ 1\end{bmatrix} \tag{6}$$

$$M_{mn}=k_{mn}\sqrt{L_mL_n};R_n=\mathrm{R}_{Cn}+R_{Sn} \tag{7}$$

where: i_0 – main path current, i_n – n-th path current, M_{mn} - m-th to n-th path mutual inductance as shown in (7), R_n - n-th path total resistance (7), R_{Cn} - n-th path equivalent contacts resistance, R_{Sn} - n-th path conductor linearized series resistance ladder-type model (Fig. 15 a). Parameters of the plate current divider circuit model for the 4-path version have been presented in Table 1. The methodology for determining the parameters has been presented below.

The model parameters values have been determined from field simulations (Fig. 8) and low-frequency current flow measurements in a real plate divider prototype (Fig. 5).

The values of self L_n and mutual M_{mn} inductances have been determined from simulation studies. Based on the simulation results, it has been determined that the maximum contribution of the internal inductance, which is the component sensitive to frequency due to the skin and the proximity effects, in the self-inductance of current paths does not exceed 8.4% over the entire range of considered frequency band. At the same time, the value of the inductance associated with the external magnetic flux (outside the conductor volume) can be considered constant within the specified frequency band. Therefore, all inductances of the model can be treated as linear parameters without introducing a significant error value.

A key problem to be considered in the construction of the circuit model in the case of transient states is the change in conductor series

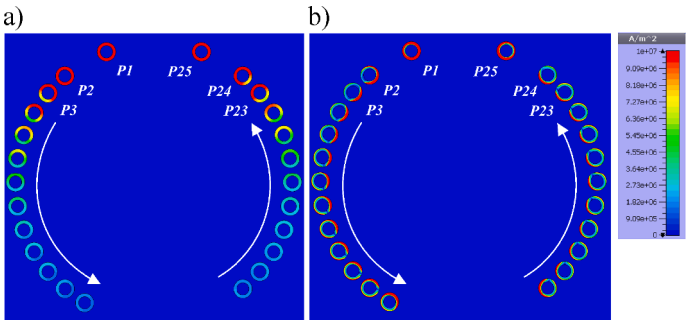

Fig. 11. Cross-sectional map of the current density vector normal component in the cylindrical divider model twenty-five paths for the excitation frequency of a) 1 Hz, and b) 10 kHz.

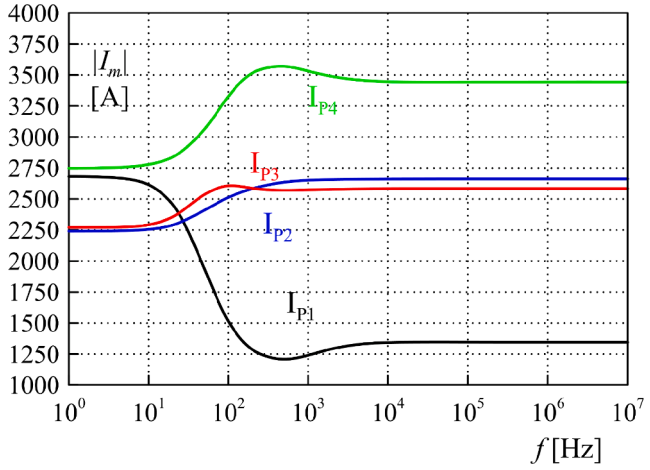

Fig. 12. Frequency characteristics of the current absolute values in individual paths of a plate divider – simulation results. Refer to Fig. 6.

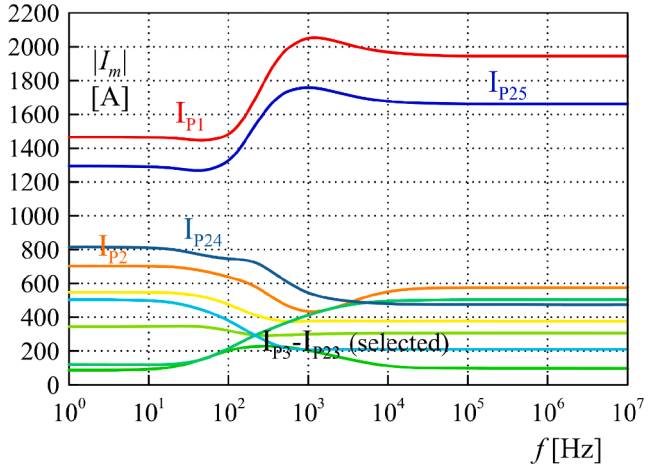

Fig. 13. Frequency characteristics of the current absolute values in individual (selected) paths of a cylindrical divider – simulation results. Refer to Fig. 7.

resistance R_{Sn} as a function of waveform slope associated with the skin and the proximity effects. There are a number of potential solutions for modelling the phenomenon of conductor current density distribution in a time domain in the literature [3,9,11–13,30,35,37]. In the proposed model, an equivalent scheme of the series component of the conductor resistance based on a seven-stage cascade LR type ladder [21,31,53] has been implemented. Field simulation described in the previous part of the article takes into account the non-linearity of the conductor resistances

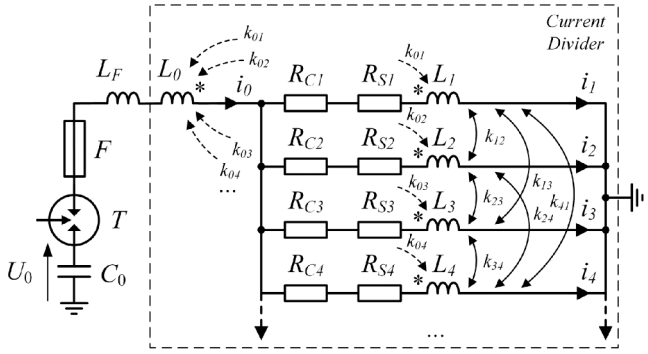

Fig. 14. Equivalent circuit model of the pulse-forming system with a multi-path current divider: $C_0 = 100$ μF – capacitance of the pulse capacitor bank; $U_0 = 10$ kV – initial capacitor voltage; T – trigatron; F – fuse; $L_F = 1.8$ μH - high voltage pulse-forming circuit inductance; L_0 – coupled part inductance of the main path; R_{Cn} – n-th path resultant contacts resistance; R_{Sn} – n-th path resultant series resistance; L_n – n-th path self-inductance; k_{0n} – main to n-th path coupling coefficient; k_{mn} – m-th to n-th path coupling coefficient.

resulting from the skin and the proximity effect, hence the adjustment of the lumped ladder parameters to the resistance frequency characteristics determined by field simulation has been performed using an iterative algorithm based on the least squares method. The schematic of the RL skin effect cascade along with the single divider path resistance frequency curve and the approximation error has been presented in Fig. 15. Approximation parameters of a single current divider path series resistance have been presented in Table 2.

The method of determining the contacts resistances R_{Cn} of the empirical Holm model and refined with the use of measurements of the low-frequency current flows in the divider branches has been presented in detail in part IV of this paper.

Current measurement compensation is based on determining the total divider current i_0 using input data in the form of an arbitrary divider path current waveform. This method takes into account the non-linear transfer characteristics of the system and eliminates the error resulting from the use of the static current ratio. The Matlab computing environment has been used to solve the system of equations (4) with linearized R_{Sn} parameters (Fig. 15 a).

The characteristics of the fitting error of the circuit model to the frequency characteristics determined on the basis of field simulation has been determined. The result of the matching has been presented in Fig. 16.

As shown in Fig. 16, the maximum value of the matching error resulting from the assumptions, including the linearity of the inductances of individual divider branches, does not exceed 8%, which is a satisfactory value.

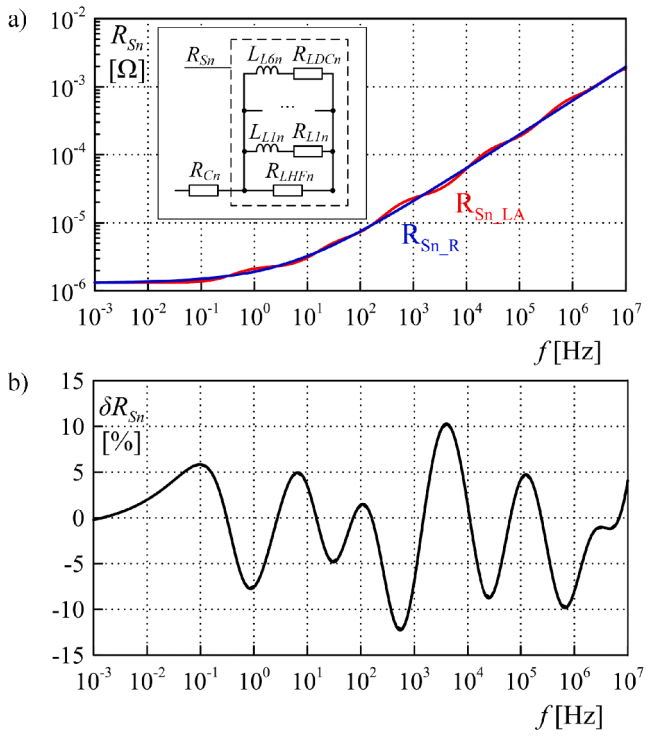

Fig. 15. Frequency characteristics of a) a series resistance LR ladder approximation R_{Sn_LA} and a field-simulation based resistance curve R_{Sn_R} along with b) a relative approximation error – simulation results.

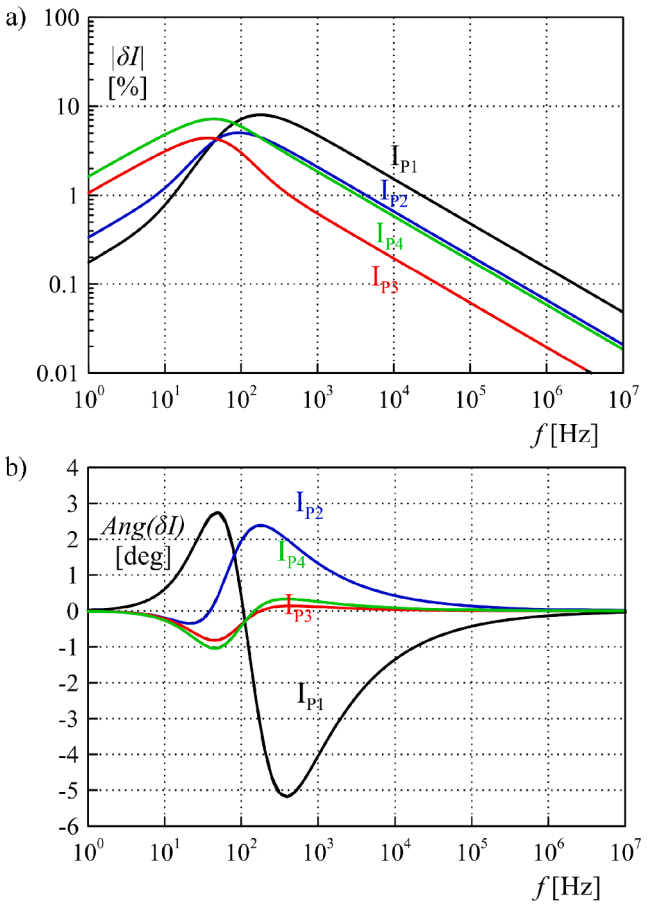

Fig. 16. Frequency characteristics of the maximum relative fitting current flow a) amplitude error, and b) phase error of the circuit current divider model to the frequency characteristics determined on the basis of field simulation.

Table 1
Circuit Model Parameters of The Plate Current Divider.

Symbol	Parameter	Value
L_0	coupled part inductance of the main path	126 nH
$L_{1\text{-}4}$	paths self-inductances	18.4 nH
R_{C1}	1st path resultant contacts resistance	27.4 μΩ
R_{C2}	2nd path resultant contacts resistance	26.7 μΩ
R_{C3}	3rd path resultant contacts resistance	31.6 μΩ
R_{C4}	4th path resultant contacts resistance	32.5 μΩ
k_{01}	main to 1st path coupling coefficient	−0.027
k_{02}	main to 2nd path coupling coefficient	0.053
k_{03}	main to 3rd path coupling coefficient	0.02
k_{04}	main to 4th path coupling coefficient	0.022
k_{12}, k_{23}, k_{34}, k_{41}	magnetic coupling coefficient of adjacent tracks	0.021
k_{13}, k_{24}	magnetic coupling coefficient of diagonal tracks	0.014

Table 2
RL Ladder Approximation Parameters of a Single Current Divider Path Conducting Resistance.

Symbol	Parameter of the n-th path	Value
R_{LHFn}	resistance for the highest considered frequency	2.2 mΩ
L_{L1n}, R_{L1n}	1st level inductance and resistance	0.104 nH, 1.5 mΩ
L_{L2n}, R_{L2n}	2nd level inductance and resistance	0.282 nH, 220 μΩ
L_{L3n}, R_{L3n}	3rd level inductance and resistance	1.31 nH, 33 μΩ
L_{L4n}, R_{L4n}	4th level inductance and resistance	11 nH, 9 μΩ
L_{L5n}, R_{L5n}	5th level inductance and resistance	59 nH, 3.5 μΩ
L_{L6n}, R_{LDCn}	6th level inductance and DC resistance	1.7 μH, 3.1 μΩ

6. Experimental verification results

In order to verify the operation of the plate current divider prototype presented in Fig. 4 and the proposed method of circuit model-based measurement results compensation, a series of experimental field tests has been carried out in a setup with an FCG and a high-power pulse-forming system, the functional diagram of which has been shown in

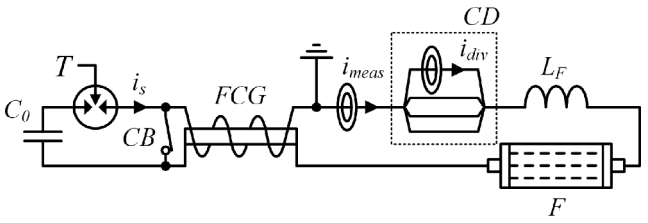

Fig. 17. Functional diagram of the high-power pulse generation and forming system experimental setup during verification tests of a plate current divider model: $C_0 = 100$ μF – capacitance of the pulse capacitor bank; T – trigatron; CB – crowbar; FCG – flux compression generator; CD – current divider model (Fig. 4); $L_F = 1.8$ μH - high voltage pulse-forming circuit coil; F – high-speed fuse-opening switch; i_s – FCG supply current; i_{meas} – FCG summary current; i_{div} – divider branch current.

Fig. 17.

A comparison of the measurement system representative summary current waveform with the result of the uncompensated scaled divider branch current and waveform determined on the basis of the compensated divider model along with the absolute both solutions error waveforms has been shown in Fig. 18.

The relative error transient value of the divider current compensated measurement based on the proposed model does not exceed 2.5% and decrease almost to zero in a steady state, compared with the value exceeding 16% without any compensation. The error remaining after the numerical compensation is probably associated with the uncertainty of the field-simulation model and measurement of the lumped elements

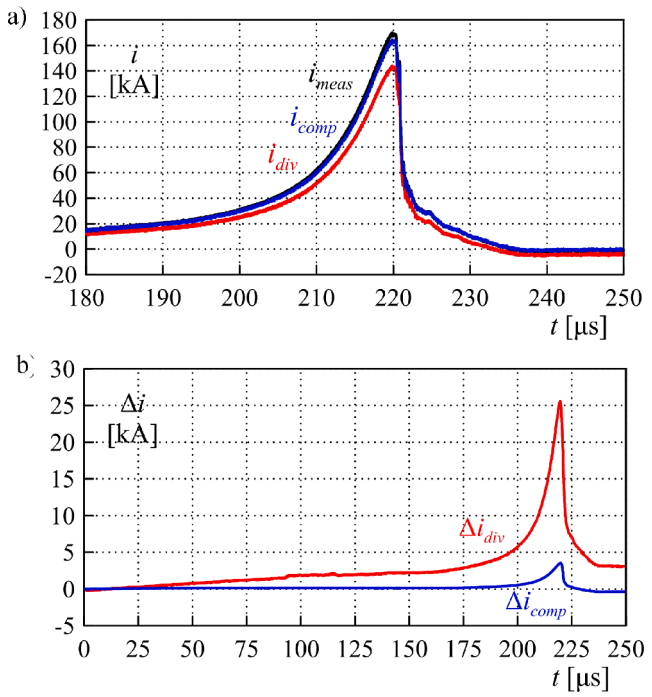

Fig. 18. Representative a) FCG summary current waveform i_{meas}, the uncompensated scaled divider branch current i_{div}, and waveform determined on the basis of the compensated divider model i_{comp} along with b) absolute error weveforms with (Δi_{comp}) and without compensation (Δi_{div}) – experimental results.

parameters of the circuit divider model, i.e. mainly the contacts resistances and the individual inductances of the divider branches. However, the obtained compensation accuracy of the current waveform is sufficient and comparable with the measurement accuracy of the current transducers themselves.

In summary, in order to increase the accuracy of current measurements with a use of any current divider, the aforementioned general design methodology can be applied as follows:

- The design of the selected topology current divider should be based on the minimum possible number of parallel paths.
- A simulation model should be prepared on the basis of which (together with basic laboratory tests of low-frequency current flows) the parameters of the equivalent circuit divider model should be determined.
- By using the model numerical solution, it is possible to compensate for the current waveform (even with a wide frequency spectrum) measured with the use of the divider.

7. Conclusions

A. The presented use of current dividers to increase the measuring range of the transducers together with appropriate numerical compensation of the results (the necessity of which results from the lack of the current flow symmetry in a wide frequency band of measured signals) is a universal measurement solution, especially useful in the field of high value and significant steepness current pulses, where transducers with the required parameters are not available.

B. The performed simulation research makes it possible to verify the design of current dividers at an early prototype stage. A proper design of the divider does not introduce significant additional inductances and parasitic resistances by using the already existing current paths fragments and structural elements.

C. The proposed general model of the current divider enables effective compensation of the results of high current pulses measurements with an error not exceeding 2.5% and decreasing almost to zero in a steady state. The lack of compensation results in an error exceeding 16%. The circuit model parameters should be determined on the basis of field simulations and low-frequency measurements of current flows in the physical prototypes of dividers.

D. In the case of a cylindrical current divider, despite the mutual symmetry of the individual current paths, the strong coupling with the main current path in the presented application makes it impossible to achieve a symmetrical flow of branches currents. The disadvantage of this solution is also a significant level of complexity of the model and numerical calculations. Hence, the general conclusion is that it is necessary to construct a divider with the lowest possible number of parallel paths, resulting from the ratio of the expected current value to the measuring range of the used transducers.

Funding

This work was supported by the Polish National Centre of Research and Development (NCBR) under project No. DOB-1-1/1/PS/2014.

CRediT authorship contribution statement

Mikołaj Nowak: Conceptualization, Methodology, Software, Validation, Formal analysis, Investigation, Resources, Writing - original draft, Writing - review & editing, Visualization. **Kazimierz Jakubiuk:** Methodology, Formal analysis, Writing - review & editing, Visualization, Supervision, Project administration, Funding acquisition. **Daniel Kowalak:** Visualization, Investigation, Validation, Writing - review & editing. **Marek Pikoń:** Conceptualization, Validation, Resources, Writing - review & editing. **Józef Czucha:** Conceptualization, Validation, Writing - review & editing. **Jacek Starzyński:** Conceptualization, Writing - review & editing.

Declaration of Competing Interest

The authors declare that they have no known competing financial interests or personal relationships that could have appeared to influence the work reported in this paper.

References

[1] "CST Studio 2018." [Online]. Available: www.cst.com.
[2] G.S.J. Argüeso, M. Robles, Measurement of high frequency currents with a Rogowski coil, Congr. Hisp. Ing Eléctrica (2005). June.
[3] F.D. Bennett, J.W. Marvin, Current measurement and transient skin effects in exploding wire circuits, Rev. Sci. Instrum. 33 (11) (1962) 1218–1226.
[4] L. Boyer, Contact resistance calculations: Generalizations of Greenwood's formula including interface films, IEEE Trans. Components Packag. Technol. 24 (1) (2001) 50–58.
[5] M. Braunovic, Effect of connection design on the contact resistance of high power overlapping bolted joints, IEEE Trans. Components Packag. Technol. 25 (4) (2002) 642–650.
[6] R. Cao, J. Li, Q. Jiao, J. Yuan, Analysis and measurement of transient currents in railgun with loop probes, IEEE Trans. Plasma Sci. 41 (5) (2013) 1479–1483.
[7] Y. Chen, Q. Huang, A.H. Khawaja, D. Cai, J. Wu, A novel non-invasion magnetic sensor array based measurement method of large current, Meas. J. Int. Meas. Confed. 139 (2019) 78–84.
[8] S. Cui, S. Wang, H. Yang, J. Yu, Research on multi-field coupling simulation of pulse current shunts, in: CPEM 2018 - Conf. Precis. Electromagn. Meas., pp. 0–1, 2018.
[9] C. Donaghy-Spargo, A. Horsfall, Transient skin effect in power electronic applications, J. Eng. 2019 (17) (2019) 3696–3700.
[10] B. Dziadak, A. Josko, J. Starzynski, Inductive sensors for stroke current and field measurements, in: Proc. 2017 18th Int. Conf. Comput. Probl. Electr. Eng. CPEE 2017, no. 1, 2017.
[11] B.E. Fridman, Skin effect in massive conductors used in pulsed electrical devices, Dig. Tech. Pap. Int. Pulsed Power Conf. 47 (9) (2002) 1112–1119.
[12] B.E. Fridman, Transients in pulsed electrical circuits with massive conductors, IEEE Trans. Plasma Sci. 34 (5 I) (2006) 1938–1943.
[13] L.J. Giacoletto, L. Fellow, Frequency- and time-domain analysis of skin effect, IEEE Trans. Magn. 32 (I) (1996) 220–229.

[14] J.A. Greenwod, J.B.P. Williamson, Contact of nominally flat surfaces, Proc. R. Soc. Lond. A. Math. Phys. Sci. 295 (1442) (1966) 300–319.
[15] M. Hamedi, M. Atashparva, A review of electrical contact resistance modeling in resistance spot welding, Weld. World 61 (2) (2017) 269–290.
[16] R.Y. Han, et al., Hybrid PCB Rogowski coil for measurement of nanosecond-risetime pulsed current, IEEE Trans. Plasma Sci. 43 (10) (2015) 3555–3561.
[17] R. Holm, Electric contacts: Theory and application, 4th ed., Springer, US, 1967.
[18] P.Y. Huang, T. Shimizu, "High power/current inductor loss measurement with shunt resistor current-sensing method", *2018 Int. Power Electron*, Conf. IPEC-Niigata - ECCE Asia (2018, 2018,) 2165–2169.
[19] K. Jakubiuk, D. Kowalak, M. Nowak, in: in *ITM Web of Conferences 19*, 2018, pp. 1–2.
[20] U. Khayam, B. Sutrisno, M. Fauzan, S. Suwarno, A. Risdiyanto, Measurement and analysis of contact resistance of new designed battery connection, in: Proc. - Jt. Int. Conf. Electr. Veh. Technol. Ind. Mech. Electr. Chem. Eng. ICEVT 2015 IMECE 2015, pp. 22–27, 2016.
[21] S. Kim, D.P. Neikirk, Compact equivalent circuit model for the skin effect, IEEE MTT-S Int. Microw. Symp. Dig. 3 (1996) 1815–1818.
[22] Y. Kim, Electromotive force analysis of current transformer during lightning surge inflow using Fourier series expansion, AIP. Adv. 7 (5) (2017).
[23] L. Kogut, K. Komvopoulos, Electrical contact resistance theory for conductive rough surfaces, J. Appl. Phys. 94 (5) (2003) 3153–3162.
[24] D. Kowalak, M. Nowak, M. Wołoszyn, K. Jakubiuk, The modeling of fuse opening switch in high-power pulse forming circuit, Prz. Elektrotechniczny 96 (2) (2020) 13–16.
[25] U. Kumar, "Performance of Rogowski coils at higher frequencies", *Order A*, J. Theory Ordered Sets Its Appl. 2010 (2010) 1–8.
[26] G.A. Kyriazis, R.M. De Souza, E.S. Yasuda, L. Di Lillo, Modeling the AC-DC transfer difference of wideband cage-type current shunts, IEEE Trans. Instrum. Meas. 69 (7) (2020) 4436–4444.
[27] J. Letosa, J.S. Artal, M. Samplón, A. Usón, F.J. Arcega, Modelization of current sensors by finite elements method, Meas. J. Int. Meas. Confed. 35 (3) (2004) 233–241.
[28] Y. Liu, T. Zhao, Y. Han, F. Lin, Core saturation detection and calibration of a current probe for fast transient currents, IEEE Sens. J. 15 (3) (2015) 1395–1403.
[29] I.A. Metwally, Coaxial-cable wound rogowski coils for measuring large-magnitude short-duration current pulses, IEEE Trans. Instrum. Meas. 62 (1) (2013) 119–128.
[30] J.H.A. Monteiro, E.C.M. Costa, A.J.G. Pinto, S. Kurokawa, O.M.O. Gatous, J. Pissolato, Simplified skin-effect formulation for power transmission lines, IET Sci. Meas. Technol. 8 (2) (2014) 47–53.
[31] B. Mukherjee, L. Wang, A. Pacelli, A practical approach to modeling skin effect in on-chip interconnects, Proc. ACM Gt. Lakes Symp. VLSI (2004) 266–270.
[32] A.P. Nurmansah, S. Hidayat, Design and testing PCB rogowski-coil current sensor for high current application, in: Int. Conf. High Volt. Eng. Power Syst. ICHVEPS 2017 - Proceeding, vol. 2017, pp. 493–497, 2017.
[33] P.A. Pearson, Transformer: US3146417, 1964.
[34] C. Romero, et al., "Measurement of lightning currents using a combination of Rogowski coils and B-dot sensors", *2010 30th Int*, Conf. Light. Prot. ICLP 2010 (2017) 71–77.
[35] A.E. Ruehli, G. Antonini, L.J. Jiang, Skin-effect loss models for time- and frequency-domain PEEC solver, Proc. IEEE 101 (2) (2013) 451–472.
[36] K. Schon, High impulse voltage and current measurement techniques, 2013.
[37] A. Services, T. Inpormahon, A.H. Station, BRL report no. 1137: Transient skin effects in exploding wire circuits, 1961.
[38] M. Shafiq, M. Lehtonen, L. Kütt, G.A. Hussain, M. Hashmi, Effect of terminating resistance on high frequency behaviour of rogowski coil for transient measurements, Elektron. ir Elektrotechnika 19 (7) (2013) 22–28.
[39] H. Shao et al., Development and applications of wideband high current transducers, in: CPEM Dig. (Conference Precis. Electromagn. Meas.), vol. 2020-Augus, pp. 2020–2021, 2020.
[40] R.M. Silva, et al., Optical Current Sensors for High Power Systems: A Review, Appl. Sci. 2 (3) (2012) 602–628.
[41] E. Thornton, Voltage and current measurement in pulsed power circuits, in: IEE Colloquium on Measurement Techniques for Power Electronics, 1991, pp. 1–4.
[42] R.S. Timsit, Electrical contact resistance: properties of stationary interfaces, IEEE Holm Conference on Electrical Contacts (1998) 1–19.
[43] S. Tumanski, Induction coil sensors - a review, Meas. Sci. Technol. 18 (3) (2007).
[44] G. Turner, I.W. Hofsajer, "Rogowski coils for short duration (<10us) pulsed current (>10kA) measurements", in: in IEEE Africon 5th Africon Conference in Africa, 1999, pp. 759–764.
[45] B. Wang, D. Wang, W. Wu, A Rogowski coil current transducer designed for wide bandwidth current pulse measurement, in: 2009 IEEE 6th Int. Power Electron. Motion Control Conf. IPEMC '09, vol. 3, pp. 1246–1249, 2009.
[46] N. Wang, Z. Zhang, Z. Li, Q. He, F. Lin, Y. Lu, Design and characterization of a low-cost self-oscillating fluxgate transducer for precision measurement of high-current, IEEE Sens. J. 16 (9) (2016) 2971–2981.
[47] S. Wang, Y. Han, M. Ding, Y. Zhao, Analysis on double-layer squirrel-cage shunt for large pulse current with high frequency, CPEM 2016 - Conf Precis. Electromagn. Meas. Conf. Dig. 1 (2016) 4–5.
[48] S. Williamson, J.W. Ralph, Finite-element analysis for nonlinear magnetic field problems with complex current sources, IEE Proc. A 129 (6) (1982) 391–395.
[49] M. Wołoszyn, D. Kowalak, K. Jakubiuk, M. Nowak, The flux compression generator load parameters selection, in: ITM Web of Conferences 28, 2019, vol. 01002, pp. 1–2.
[50] Y. Xu, X. Zou, X. Wang, Influencing factors and error analysis of pulse current measurement with air-core rogowski coil, IEEE Trans. Plasma Sci. 48 (12) (2020) 4381–4386.
[51] C. Yao, Q. Xiao, Y. Mi, T. Yuan, C. Li, W. Sima, Contactless measurement of lightning current using self-integrating B-dot probe, IEEE Trans. Dielectr. Electr. Insul. 18 (4) (2011) 1323–1327.
[52] W. Ye, Z. Dong, R. Ren, J. Liu, K. Huang, C. Zhang, Application research on fiber-optic current sensor in large pulse current measurement,, J. Phys. Conf. Ser. 1507 (7) (2020).
[53] H.S. Yen, Z. Fazarinc, R.L. Wheeler, Time-Domain Skin-Effect Model for Transient Analysis of Lossy Transmission Lines, Proc. IEEE 70 (7) (1982) 750–757.
[54] Y. Zeroukhi, E. Napieralska-Juszczak, G. Vega, K. Komeza, F. Morganti, S. Wiak, Dependence of the contact resistance on the design of stranded conductors, Sensors (Switzerland) 14 (8) (2014) 13925–13942.
[55] M. Zhang, K. Li, S. He, J. Wang, Design and test of a new high-current electronic current transformer with a rogowski coil, Metrol. Meas. Syst. XXI (1) (2014) 121–132.
[56] Y. Zhang, J. Liu, G. Bai, J. Feng, Analysis of damping resistor's effects on pulse response of self-integrating Rogowski coil with magnetic core, Meas. J. Int. Meas. Confed. 45 (5) (2012) 1277–1285.